

Observation of Non-Bloch Parity-Time Symmetry and Exceptional Points

Lei Xiao,^{1,*} Tianshu Deng,^{2,*} Kunkun Wang,¹ Zhong Wang,^{2,†} Wei Yi,^{3,4,‡} and Peng Xue^{1,§}

¹Beijing Computational Science Research Center, Beijing 100084, China

²Institute for Advanced Study, Tsinghua University, Beijing 100084, China

³CAS Key Laboratory of Quantum Information, University of Science and Technology of China, Hefei 230026, China

⁴CAS Center For Excellence in Quantum Information and Quantum Physics, Hefei 230026, China



(Received 13 January 2021; accepted 29 April 2021; published 10 June 2021)

Parity-time (PT)-symmetric Hamiltonians have widespread significance in non-Hermitian physics. A PT -symmetric Hamiltonian can exhibit distinct phases with either real or complex eigenspectrum, while the transition points in between, the so-called exceptional points, give rise to a host of critical behaviors that holds great promise for applications. For spatially periodic non-Hermitian systems, PT symmetries are commonly characterized and observed in line with the Bloch band theory, with exceptional points dwelling in the Brillouin zone. Here, in nonunitary quantum walks of single photons, we uncover a novel family of exceptional points beyond this common wisdom. These “non-Bloch exceptional points” originate from the accumulation of bulk eigenstates near boundaries, known as the non-Hermitian skin effect, and inhabit a generalized Brillouin zone. Our finding opens the avenue toward a generalized PT -symmetry framework, and reveals the intriguing interplay between PT symmetry and non-Hermitian skin effect.

DOI: [10.1103/PhysRevLett.126.230402](https://doi.org/10.1103/PhysRevLett.126.230402)

While Hermiticity of Hamiltonians is a fundamental axiom in the standard quantum mechanics for closed systems, non-Hermitian Hamiltonians arise in open systems and possess unique features. Particularly, a wide range of non-Hermitian Hamiltonians, protected by the parity-time (PT) symmetry, can have entirely real eigenvalues [1–4]. A PT -symmetric Hamiltonian generally has two phases, the exact PT phase and the broken PT one, with real and complex eigenenergies, respectively. The transition points between these phases are called exceptional points, on which eigenstates and eigenenergies coalesce while the Hamiltonian becomes nondiagonalizable. PT symmetry and exceptional points are ubiquitous in non-Hermitian systems, and lead to dramatic consequences and promising applications such as unidirectional invisibility [5], single-mode lasers [6,7], enhanced sensing [8,9], topological energy transfer [10], and nonreciprocal wave propagation [11,12], to name just a few. In practice, physical systems with PT symmetry are often based on spatially periodic structures (e.g., photonic lattices or microwave arrays) [2,13], where the notion of Bloch band greatly simplifies their characterization as each Bloch wave is treated independently.

Here we uncover a novel class of exceptional points beyond this Bloch-band picture in periodic systems. This work is partially stimulated by recent discoveries of non-Hermitian topological systems whose topological properties are highly sensitive to boundary conditions, in sharp contrast to their Hermitian counterparts. Specifically, for a generic family of non-Hermitian systems under the open-boundary condition (OBC), all eigenstates accumulate near the boundaries, whereas they always behave as extended

Bloch waves under a periodic boundary condition (PBC). This phenomenon, known as the non-Hermitian skin effect, invalidates the conventional bulk-boundary correspondence and necessitates a redefinition of topological invariants [14–18]. Whereas topological physics has been the focus in previous studies [19–25], a fundamental question remains whether the non-Hermitian skin effect has significant consequences beyond topology, among which the interplay of non-Hermitian skin effect and PT symmetry is arguably the most intriguing [26,27]. In this work, we experimentally observe exceptional points generated by the non-Hermitian skin effect. Despite a translationally invariant bulk, the observed exceptional points exist in a “generalized Brillouin zone” (GBZ) [19,20,22,26,27] (rather than the standard Brillouin zone), thus representing an unexplored class of exceptional points beyond the conventional Bloch-band framework. Just as the framework with conventional Bloch bands has been commonly adopted to describe periodic lattices in physical systems ranging from condensed matter to photonics, the generalized mechanism of PT symmetry, confirmed by our observation of “non-Bloch exceptional points,” is relevant to a broad class of non-Hermitian platforms with periodic structures.

In general, a discrete-time, nonunitary quantum walk can be characterized by $|\psi(t)\rangle = U^t|\psi(0)\rangle$ ($t = 0, 1, 2, \dots$), which amounts to a stroboscopic simulation of the time evolution with initial state $|\psi(0)\rangle$, and generated by the non-Hermitian effective Hamiltonian H_{eff} with $U := e^{-iH_{\text{eff}}}$. To be concrete, we take the following one-dimensional Floquet operator

$$U = R\left(\frac{\theta_1}{2}\right)S_2R\left(\frac{\theta_2}{2}\right)MR\left(\frac{\theta_2}{2}\right)S_1R\left(\frac{\theta_1}{2}\right), \quad (1)$$

where the shift operators, $S_1 = \sum_x |x\rangle\langle x| \otimes |0\rangle\langle 0| + |x+1\rangle\langle x| \otimes |1\rangle\langle 1|$ and $S_2 = \sum_x |x-1\rangle\langle x| \otimes |0\rangle\langle 0| + |x\rangle\langle x| \otimes |1\rangle\langle 1|$, selectively shift the walker along a one-dimensional lattice (with lattice sites labeled by x) in a direction that depends on its internal coin state $|0\rangle(|1\rangle)$, the $+1$ (-1) eigenstate of the Pauli matrix σ_z . The coin operator $R(\theta) = \mathbb{1}_w \otimes e^{-i\theta\sigma_y}$, with $\mathbb{1}_w = \sum_x |x\rangle\langle x|$, rotates coin states without shifting the walker position. The gain and loss is implemented by $M = \mathbb{1}_w \otimes e^{\gamma\sigma_z}$.

We implement the quantum walk using a single-photon interferometric network [Fig. 1(a)], where coin states $|0\rangle$ and $|1\rangle$ are encoded in the horizontal and vertical photon polarizations, respectively. Rotations of the coin states (R) are implemented by HWPs. Shift operators $S_{1,2}$ are realized by beam displacers that allow the transmission of vertically polarized photons while displacing horizontally polarized ones into neighboring positions. Finally, the gain/loss is implemented by a PPBS, which reflects state $|1\rangle$ with a probability p , and directly transmits state $|0\rangle$. Thus, the PPBS realizes $M_E = \mathbb{1}_w \otimes (|0\rangle\langle 0| + \sqrt{1-p}|1\rangle\langle 1|)$, which is related to M as $M = e^{\gamma}M_E$, with $\gamma = -(1/4)\ln(1-p)$. We therefore readout $|\psi(t)\rangle$ from our experiment with M_E by adding a factor $e^{\gamma t}$. More details of our experimental setup can be found in [28].

Under the Floquet operator U , the directional hopping in $S_{1,2}$ and the gain/loss in M conspire to generate

non-Hermitian skin effect [15]. When a domain wall is created between two regions with different parameters, e.g., $\theta_{1,2}^L$ and $\theta_{1,2}^R$ for the left and right regions in Fig. 1(b), all the eigenstates of U are localized at the domain wall [15]. While the non-Hermitian skin effect dramatically affects topological properties, here we focus on the impact of non-Hermitian skin effect on the emergence of PT symmetry and exceptional points.

The exact (broken) PT phase corresponds to the absence (presence) of nonzero imaginary parts in the eigen spectrum (quasienergies) of H_{eff} . Note that we use these terms in a general sense, including pseudo-Hermiticity whose role is, regarding spectral reality, similar to the original PT symmetry [29,30]. In Figs. 2(a), 2(b), we show in blue the calculated imaginary parts of quasienergies, $\text{Im}(E)$, for the domain-wall geometry with OBC at the two ends [see Fig. 1(b)]. For both Figs. 2(a), 2(b), an exceptional point is found as θ_2^R is varied while fixing other parameters. Remarkably, the exceptional point cannot be deduced from the Bloch band theory. The Bloch theory suggests that the continuous bulk spectra of U under the domain-wall geometry are the union of the spectra corresponding to the left and right bulks, which are respectively obtained from the Bloch Floquet operator $U(k)$ ($k \in [0, 2\pi]$, i.e., within the standard Brillouin zone) associated with the left (with parameters $\theta_{1,2}^L$) and right (with $\theta_{1,2}^R$) bulk. These spectra are shown in gray in Figs. 2(a), 2(b), which dramatically differ from the actual (non-Bloch) spectra under the domain-wall geometry.

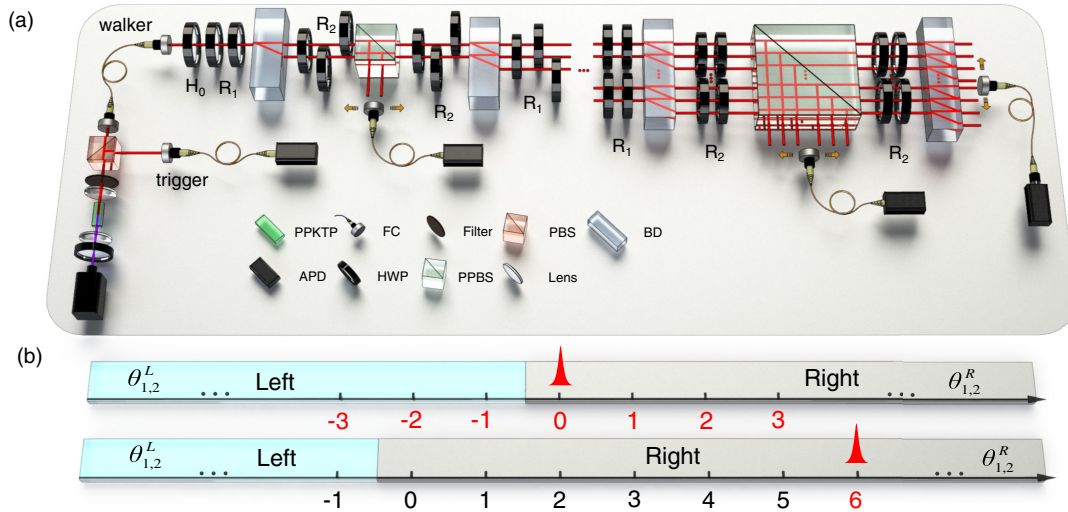


FIG. 1. Experimental implementation. (a) A pair of photons is generated via the spontaneous parametric down conversion in the periodically poled potassium titanyl phosphate crystal (PPKTP), with one serving as a trigger and the other (walker) projected into the quantum-walk network as the walker photon. After passing through a polarizing beam splitter (PBS) and a half-wave plate (HWP), the polarization of the walker photon is initialized as $|0\rangle$. It then undergoes a quantum walk through an interferometric network, composed of HWPs, beam displacers (BDs), and partially polarizing beam splitter (PPBS), and is finally detected by avalanche photodiodes (APDs), in coincidence with the trigger photon. (b) The domain-wall geometry of non-Hermitian quantum walks. Upper panel (scheme I): the walker starts near the domain wall at $x = 0$. Lower panel (scheme II): the walker starts from the bulk (i.e., far away from the domain wall) position $x = 6$.

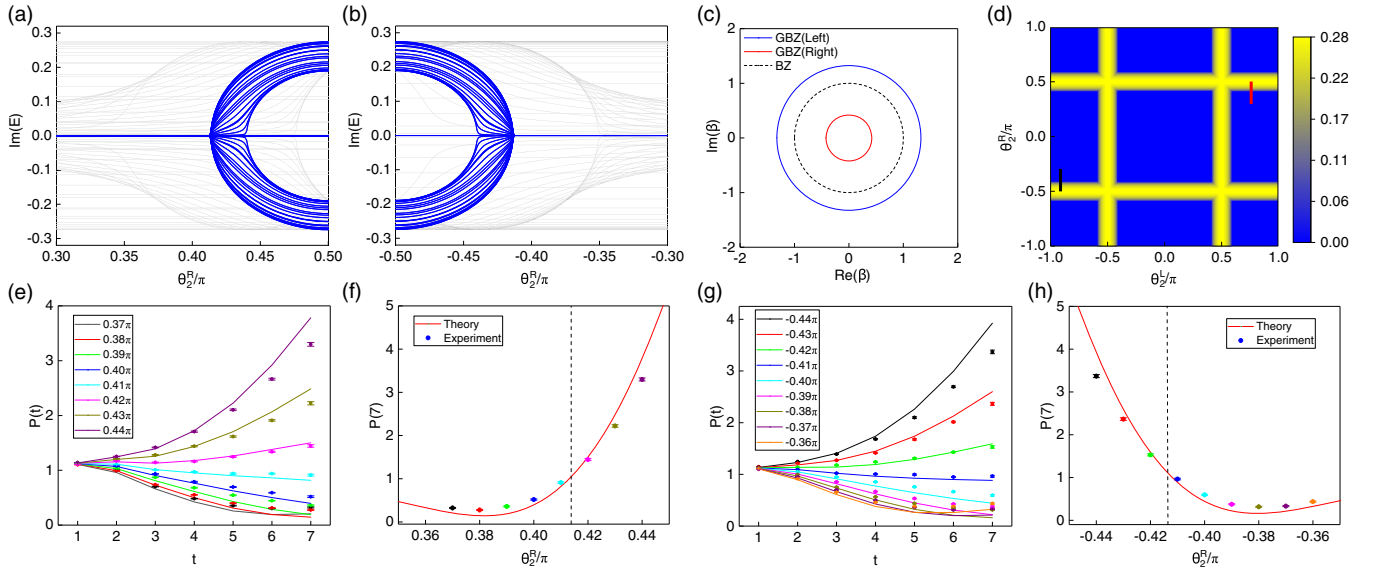


FIG. 2. Non-Bloch exceptional points from domain-wall measurements. (a), (b) Imaginary part of quasienergies, $\text{Im}(E)$ versus θ_2^R . Other coin parameters are fixed at $\theta_1^R = 0.5625\pi$ and $\theta_1^L = -0.0625\pi$. We take $\theta_2^L = 0.75\pi$ and -0.9735π for (a) and (b), respectively. Blue and gray lines represent the OBC (non-Bloch) and PBC (Bloch) spectra, respectively. The blue non-Bloch spectra feature an exceptional point at $|\theta_2^R| = 0.413\pi$, while the gray Bloch spectra remain complex-valued throughout. (c) Brillouin zone and GBZ for $\theta_1^R = 0.5625\pi$, $\theta_1^L = -0.0625\pi$, $\theta_2^R = -0.44\pi$, and $\theta_2^L = -0.9735\pi$. (d) Numerically calculated $\max[\text{Im}(E)]$ for $\theta_1^R = 0.5625\pi$ and $\theta_1^L = -0.0625\pi$. The yellow (blue) region is the broken (exact) PT phase. The red and black cuts correspond to (a), (e), (f) and (b), (h), respectively. (e) Experimentally measured $P(t)$ (symbols) with an initial state $|\psi(t=0)\rangle = |0\rangle_x \otimes |0\rangle_{\text{coin}}$ up to seven steps for eight different values of θ_2^R , together with the theoretical predictions (curves). Other coin parameters are the same as in (a), e.g., $\theta_2^L = 0.75\pi$. (f) $P(t=7)$ under the same parameters as those in (c). Error bars indicate the statistical uncertainty obtained by assuming Poissonian statistics. The red line is plotted from numerical simulations of seven-step evolutions, from which the exceptional point is predicted to be $\theta_2^R = 0.413\pi$ [by requiring $P(7) = 1$], consistent with the theoretical prediction from Eq. (3). (g), (h) The same as (e), (f) except that $\theta_2^L = -0.9735\pi$. From the numerical simulations (red line), the exceptional point in (h) is at $\theta_2^R = -0.412\pi$. The loss parameter is fixed at $\gamma = 0.2746$ throughout our experiment.

This discrepancy is due to the aforementioned non-Hermitian skin effect. The exponential decay of eigenstates in the real space means that the Bloch phase factor e^{ik} , which corresponds to extended plane waves, should be replaced by a factor β ($|\beta| \neq 1$ in general) in order to generate the eigenspectra under the OBC. Furthermore, β must belong to a closed loop in the complex plane, dubbed the GBZ [19,22], which typically deviates from the unit circle [Fig. 2(c)]. For $\beta \in \text{GBZ}$, eigenenergies under the OBC are recovered by performing the analytic continuation $U(k)|_{e^{ik} \rightarrow \beta}$, and taking the logarithm of eigenvalues of $U(\beta)$. Crucially, we find that $U(\beta)$ satisfies the η -pseudo-unitarity

$$\eta U^{-1}(\beta) \eta^{-1} = U^\dagger(\beta)|_{\beta \in \text{GBZ}}, \quad (2)$$

when $|\cos \theta_2^{L(R)}| > |\tanh \gamma|$ [28]. Here $\eta = \sum_n |\chi_n\rangle\langle \chi_n|$, where $\{|\chi_n\rangle\}$ is the collection of left eigenstates of $U(\beta)$. Equation (2) corresponds to the η -pseudo-Hermiticity of the non-Hermitian effective Hamiltonian: $\eta H_{\text{eff}}(\beta) \eta^{-1} = H_{\text{eff}}^\dagger(\beta)$ [29,30], which is a generalization of the PT symmetry, and guarantees the reality of quasienergies as

long as the relation holds. As such, the GBZ theory predicts non-Bloch exceptional points at

$$|\cos \theta_2^{L(R)}| = |\tanh \gamma|. \quad (3)$$

We observe exceptional points by probing probabilities of the photon surviving in the quantum walk after each time step t , which are constructed from photon-number measurements up to t [28]. They are then multiplied by a factor $e^{2\gamma t}$ (due to the aforementioned difference between M_E and M) to yield the corrected probability $P(t)$ that corresponds to the wave function norm, whose long-time behavior is $P(t) = \langle \psi(t) | \psi(t) \rangle \sim e^{2 \max[\text{Im}(E)] t}$. Therefore, an exponential growth of $P(t)$ indicates the broken PT phase. By contrast, $P(t)$ in the exact PT phase typically approaches a steady-state value of order of unity. Such a feature enables us to extract the location of exceptional points by tracking the time evolution of the corrected probability. Experimentally, this is achieved through two schemes: (I) the domain wall scheme and (II) the bulk scheme.

In the first scheme, we initiate the photon walker near the domain wall, as illustrated in the upper panel of Fig. 1(b),

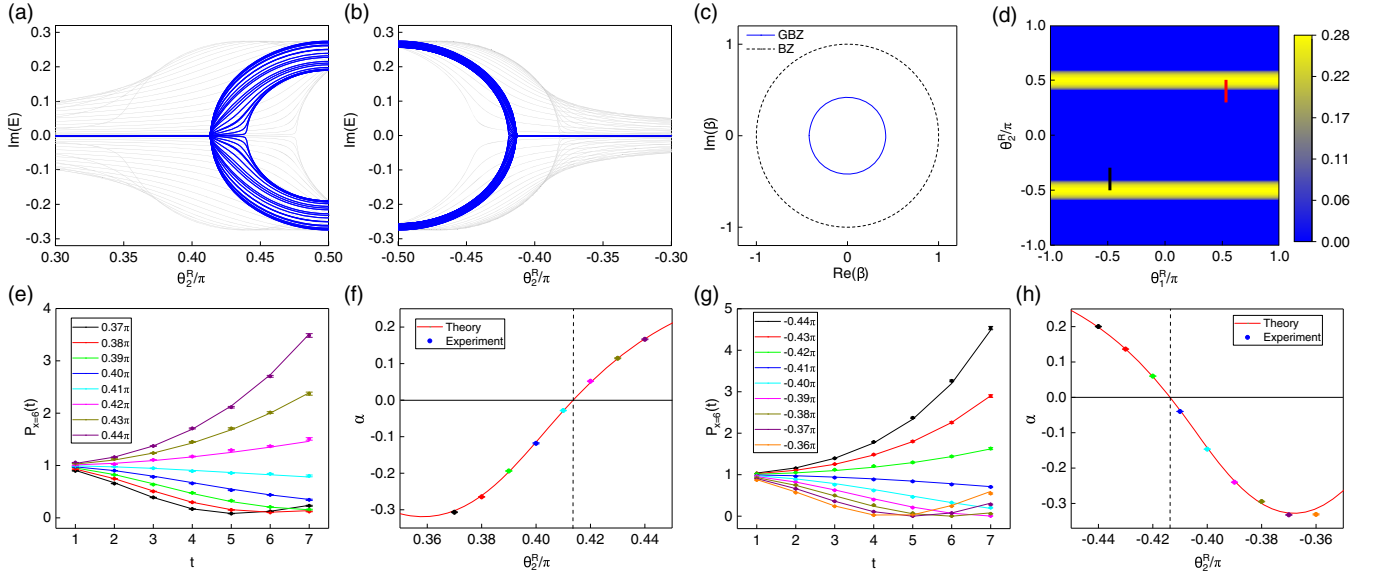


FIG. 3. Non-Bloch exceptional points from bulk measurements. (a) $\text{Im}(E)$ versus θ_2^R , with $\theta_1^R = 0.5625\pi$ fixed. (b) $\text{Im}(E)$ versus θ_2^R , with $\theta_1^R = -0.4688\pi$ fixed. (c) GBZ of the right region, for $\theta_1^R = -0.4688\pi$ and $\theta_2^R = -0.44\pi$. (d) Numerically calculated $\max[\text{Im}(E)]$. The blue and yellow regions correspond to the exact and broken PT phase, respectively. (e) Experimentally measured $P_{x=6}(t)$ (symbols) with an initial state $|\psi(0)\rangle = |6\rangle_x \otimes |0\rangle_{\text{coin}}$ for eight values of θ_2^R , compared to the theoretical predictions (curves). Here we fix $\theta_1^R = 0.5625\pi$. (f) Exponent α versus θ_2^R extracted from the data in (e). The red line is plotted from numerical simulations of seven-step evolutions, from which the exceptional point is predicted to be $\theta_2^R = 0.414\pi$ (by requiring $\alpha = 0$), consistent with the theoretical prediction from Eq. (3). (g), (h) The same as (e), (f), except that $\theta_1^R = -0.5\pi$. (e), (f) and (g), (h) correspond to the red and black cuts in the phase diagram (d), respectively. From the numerical simulation (red line), the exceptional point in (h) is at $\theta_2^R = -0.414\pi$. The left region is idle throughout measurements, which are performed in the right region only. Without loss of generality, we take $\theta_1^L = -0.0625\pi$ and $\theta_2^L = 0.75\pi$ for (e), (f), and $\theta_1^L = -0.0625\pi$ and $\theta_2^L = -0.9375\pi$ for (g), (h).

with the initial state $|\psi(t=0)\rangle = |0\rangle_x \otimes |0\rangle_{\text{coin}}$. We then measure the corrected probability along the red and black cuts in the numerically simulated phase diagram [Fig. 2(d)], where the blue and yellow regions correspond to the exact and broken PT phase, respectively. In Fig. 2(e) (red cut), $P(t)$ grows with t for $\theta_2^R \geq 0.42\pi$ and decreases for $\theta_2^R \leq 0.41\pi$. Therefore, we infer the presence of an exceptional point between $\theta_2^R = 0.41\pi$ and 0.42π . This is consistent with Eq. (3), which predicts an exceptional point at $\theta_2^R = \pm 0.413\pi$. We arrive at the same conclusion by measuring corrected probabilities at the time step $t = 7$ [Fig. 2(f)], which become prominently larger than 1 in the broken PT phase. Similarly, Figs. 2(g), 2(h) (blue cut) indicate an exceptional point in the region $\theta_2^R \in [-0.42\pi, -0.41\pi]$, again consistent with Eq. (3).

The second scheme is based on local measurements in the bulk. The walker starts from a position $x = x_0$ far from the domain wall [Fig. 1(b), lower panel], and the subsequent corrected probability at $x = x_0$, i.e., $P_{x_0}(t) = |\langle 0 | \otimes \langle x_0 | \psi(t) \rangle|^2 + |\langle 1 | \otimes \langle x_0 | \psi(t) \rangle|^2$, is measured. In the broken PT phase, the corrected probability grows as $P_{x_0}(t) \propto e^{\alpha t}$, where $\alpha > 0$ is given by the imaginary part of quasienergies at certain special points of the GBZ [26,27]. In the exact PT phase, by contrast, $P_{x_0}(t)$ features an oscillatory behavior at short times, enveloped by an overall

decay characterized by $\alpha < 0$ (which approaches zero as the evolution time increases) [27,28]. In our experiment, we fix $x_0 = 6$ in the right region, leaving the left region idle. The imaginary parts of quasienergy spectra under OBC are plotted in Figs. 3(a), 3(b), along the red and black cuts in Fig. 3(d), respectively. The spectra are calculated by diagonalizing $U(\beta)|_{\beta \in \text{GBZ}}$ for the right region, with GBZ shown in Fig. 3(c). Along the red cut ($\theta_1^R = 0.5625\pi$), the measured $P_{x=6}(t)$ exhibits growth for $\theta_2^R \geq 0.42\pi$, and decreases for $\theta_2^R \leq 0.41\pi$ as illustrated in Fig. 3(e), indicating an exceptional point within $[0.41\pi, 0.42\pi]$. This is consistent with Fig. 3(a). Moreover, we fit $P_{x=6}(t)$ exponentially in Fig. 3(f). While the accuracy in α is limited by the small number of experimentally feasible steps [28], the fitted α does yield qualitatively consistent results: the sign of α is positive (negative) in the broken (exact) PT phase. A similar exceptional point is observed along the black cut ($\theta_1^R = -0.5\pi$) in Figs. 3(g), 3(h).

Notably, under the bulk scheme, we are able to establish non-Bloch PT symmetry and detect non-Bloch exceptional points from dynamics purely in the bulk, i.e., essentially under PBC. This highlights the observed non-Bloch exceptional points as intrinsic properties of our system, rather than mere finite-size effects. While we have revealed the non-Bloch PT transition using a seven-step quantum walk,

alternative designs (such as the time-multiplexed framework [31]) with the potential of achieving a longer evolution time would enable a more precise probe of the transition, including accurate determination of the Lyapunov exponent [26,27].

The significance of the observed non-Bloch PT symmetry and exceptional points is further enhanced by the following generic finding: in the presence of non-Hermitian skin effect, the Bloch energy spectra (calculated from the Brillouin zone) can never have PT symmetry. In fact, recent theoretical works prove that, if a system features non-Hermitian skin effect under the OBC, the associated Bloch spectra must form loops in the complex plane [32–34]. However, looplike spectra cannot lie in the real axis, thus forbidding entirely real spectrum. In sharp contrast, the non-Bloch spectra calculated from the GBZ, which correctly reflect eigenenergies under the experimentally relevant OBC, form arcs or lines enclosing no area. Real spectra and PT symmetry are henceforth enabled. Therefore, non-Bloch PT symmetry is the only general mechanism for achieving PT symmetry in the presence of non-Hermitian skin effect.

The observed interplay between non-Hermitian skin effect and PT symmetry underlines a fundamentally new mechanism for PT symmetry and exceptional points in periodic systems, and demonstrates the power of non-Bloch band theory beyond topology. Since both the non-Hermitian skin effect and PT symmetry are generic features of a large class of non-Hermitian systems, the mechanism is general and applies to a variety of non-Hermitian platforms ranging from photonic lattices to cold atoms. In view of the potential utilities of exceptional points, the non-Bloch exceptional points observed here would inspire novel designs and applications such as enhanced sensing with interface-sensitive, ultrahigh spatial resolutions [8,9,16], or robust wireless power transfer that are tunable by the interface geometry [35].

This work has been supported by the National Natural Science Foundation of China (Grants No. 12025401, No. 11674189, No. U1930402, and No. 11974331) and a start-up fund from the Beijing Computational Science Research Center. W. Y. acknowledges support from the National Key Research and Development Program of China (Grants No. 2016YFA0301700 and No. 2017YFA0304100). K. W. and L. X. acknowledge support from the Project Funded by China Postdoctoral Science Foundation (Grants No. 2019M660016 and No. 2020M680006).

*These authors contributed equally to this work

[†]wangzhongemail@tsinghua.edu.cn

[‡]wyiz@ustc.edu.cn

[§]gnep.eux@gmail.com

[1] C. M. Bender and S. Boettcher, Real Spectra in Non-Hermitian Hamiltonians Having PT Symmetry, *Phys. Rev. Lett.* **80**, 5243 (1998).

- [2] R. El-Ganainy, K. G. Makris, M. Khajavikhan, Z. H. Musslimani, S. Rotter, and D. N. Christodoulides, Non-Hermitian physics and PT symmetry, *Nat. Phys.* **14**, 11 (2018).
- [3] Ş. K. Özdemir, S. Rotter, F. Nori, and L. Yang, Parity–time symmetry and exceptional points in photonics, *Nat. Mater.* **18**, 783 (2019).
- [4] M. A. Miri and A. Alù, Exceptional points in optics and photonics, *Science* **363**, eaar7709 (2019).
- [5] A. Regensburger, C. Bersch, M. A. Miri, G. Onishchukov, D. N. Christodoulides, and U. Peschel, Parity–time synthetic photonic lattices, *Nature (London)* **488**, 167 (2012).
- [6] L. Feng, Z. J. Wong, R. M. Ma, Y. Wang, and X. Zhang, Single-mode laser by parity-time symmetry breaking, *Science* **346**, 972 (2014).
- [7] H. Hodaei, M. A. Miri, M. Heinrich, D. N. Christodoulides, and M. Khajavikhan, Parity-time–symmetric microring lasers, *Science* **346**, 975 (2014).
- [8] W. Chen, Ş. K. Özdemir, G. Zhao, J. Wiersig, and L. Yang, Exceptional points enhance sensing in an optical microcavity, *Nature (London)* **548**, 192 (2017).
- [9] H. Hodaei, A. U. Hassan, S. Wittek, H. Garcia-Gracia, R. El-Ganainy, D. N. Christodoulides, and M. Khajavikhan, Enhanced sensitivity at higher-order exceptional points, *Nature (London)* **548**, 187 (2017).
- [10] H. Xu, D. Mason, L. Jiang, and J. G. E. Harris, Topological energy transfer in an optomechanical system with exceptional points, *Nature (London)* **537**, 80 (2016).
- [11] C. E. Rüter, K. G. Makris, R. El-Ganainy, D. N. Christodoulides, M. Segev, and D. Kip, Observation of parity–time symmetry in optics, *Nat. Phys.* **6**, 192 (2010).
- [12] B. Peng, Ş. K. Özdemir, F. Lei, F. Monifi, M. Gianfreda, G. L. Long, S. H. Fan, F. Nori, C. M. Bender, and L. Yang, Parity–time–symmetric whispering-gallery microcavities, *Nat. Phys.* **10**, 394 (2014).
- [13] K. G. Makris, R. El-Ganainy, D. N. Christodoulides, and Z. H. Musslimani, Beam Dynamics in PT Symmetric Optical Lattices, *Phys. Rev. Lett.* **100**, 103904 (2008).
- [14] T. Helbig, T. Hofmann, S. Imhof, M. Abdelghany, T. Kiessling, L. W. Molenkamp, C. H. Lee, A. Szameit, M. Greiter, and R. Thomale, Generalized bulk-boundary correspondence in non-Hermitian topoelectrical circuits, *Nat. Phys.* **16**, 747 (2020).
- [15] L. Xiao, T. Deng, K. Wang, G. Zhu, Z. Wang, W. Yi, and P. Xue, Non-Hermitian bulk-boundary correspondence in quantum dynamics, *Nat. Phys.* **16**, 761 (2020).
- [16] S. Weidemann, M. Kremer, T. Helbig, T. Hofmann, A. Stegmaier, M. Greiter, R. Thomale, and A. Szameit, Topological funneling of light, *Science* **368**, 311 (2020).
- [17] A. Ghatak, M. Brandenbourger, J. van Wezel, and C. Coulais, Observation of non-Hermitian topology and its bulk–edge correspondence in an active mechanical metamaterial, *Proc. Natl. Acad. Sci. U.S.A.* **117**, 29561 (2020).
- [18] T. Hofmann, T. Helbig, F. Schindler, N. Salgo, M. Brzezińska, M. Greiter, T. Kiessling, D. Wolf, A. Vollhardt, A. Kabaši, C. H. Lee, A. Bilušić, R. Thomale, and T. Neupert, Reciprocal skin effect and its realization in a topoelectrical circuit, *Phys. Rev. Research* **2**, 023265 (2020).
- [19] S. Yao and Z. Wang, Edge States and Topological Invariants of Non-Hermitian Systems, *Phys. Rev. Lett.* **121**, 086803 (2018).

- [20] S. Yao, F. Song, and Z. Wang, Non-Hermitian Chern Bands, *Phys. Rev. Lett.* **121**, 136802 (2018).
- [21] F. K. Kunst, E. Edvardsson, J. C. Budich, and E. J. Bergholtz, Biorthogonal Bulk-Boundary Correspondence in Non-Hermitian Systems, *Phys. Rev. Lett.* **121**, 026808 (2018).
- [22] K. Yokomizo and S. Murakami, Non-Bloch Band Theory of Non-Hermitian Systems, *Phys. Rev. Lett.* **123**, 066404 (2019).
- [23] C. H. Lee and R. Thomale, Anatomy of skin modes and topology in non-Hermitian systems, *Phys. Rev. B* **99**, 201103(R) (2019).
- [24] K. Kawabata, K. Shiozaki, M. Ueda, and M. Sato, Symmetry and Topology in Non-Hermitian Physics, *Phys. Rev. X* **9**, 041015 (2019).
- [25] V. M. Martinez Alvarez, J. E. Barrios Vargas, and L. E. F. Foa Torres, Non-Hermitian robust edge states in one dimension: Anomalous localization and eigenspace condensation at exceptional points, *Phys. Rev. B* **97**, 121401(R) (2018).
- [26] S. Longhi, Probing non-Hermitian skin effect and non-Bloch phase transitions, *Phys. Rev. Research* **1**, 023013 (2019).
- [27] S. Longhi, Non-Bloch PT symmetry breaking in non-Hermitian photonic quantum walks, *Opt. Lett.* **44**, 5804 (2019).
- [28] See the Supplemental Material at <http://link.aps.org/supplemental/10.1103/PhysRevLett.126.230402> for details on experimental methods, quasienergy spectrum, characterization of non-Bloch PT symmetry in the generalized Brillouin zone, as well as additional experimental and numerical data.
- [29] A. Mostafazadeh, Pseudo-Hermiticity versus PT symmetry: The necessary condition for the reality of the spectrum of a non-Hermitian Hamiltonian, *J. Math. Phys. (N.Y.)* **43**, 205 (2002).
- [30] A. Mostafazadeh, Pseudo-Hermiticity versus PT-symmetry. II. A complete characterization of non-Hermitian Hamiltonians with a real spectrum, *J. Math. Phys. (N.Y.)* **43**, 2814 (2002).
- [31] C. Chen, X. Ding, J. Qin, Y. He, Y. H. Luo, M. C. Chen, C. Liu, X. L. Wang, W. J. Zhang, H. Li, L. X. You, Z. Wang, D. W. Wang, B. C. Sanders, C. Y. Lu, and J. W. Pan, Observation of Topologically Protected Edge States in a Photonic Two-Dimensional Quantum Walk, *Phys. Rev. Lett.* **121**, 100502 (2018).
- [32] K. Zhang, Z. Yang, and C. Fang, Correspondence between Winding Numbers and Skin Modes in Non-Hermitian Systems, *Phys. Rev. Lett.* **125**, 126402 (2020).
- [33] N. Okuma, K. Kawabata, K. Shiozaki, and M. Sato, Topological Origin of Non-Hermitian Skin Effects, *Phys. Rev. Lett.* **124**, 086801 (2020).
- [34] C. H. Lee, L. Li, R. Thomale, and J. Gong, Unraveling non-hermitian pumping: Emergent spectral singularities and anomalous responses, *Phys. Rev. B* **102**, 085151 (2020).
- [35] S. Assaworarith, X. Yu, and S. Fan, Robust wireless power transfer using a nonlinear parity-time-symmetric circuit, *Nature (London)* **546**, 387 (2017).